

# Highly transparent and strong nanohesive hydrogel patch for tissue adhesion

Qing Luo<sup>1,2</sup>, Zhao Pan<sup>2</sup>, Yong-Hong Song<sup>3</sup>, Jie-Yu Huang<sup>1,2</sup>, Hui Fang<sup>4</sup>, Dong-Quan Liu<sup>5</sup>✉, and Liang Dong<sup>2</sup>✉

<sup>1</sup>College of Materials Science and Engineering, Zhejiang University of Technology, Hangzhou 310014, China;

<sup>2</sup>Zhejiang Cancer Hospital, Hangzhou Institute of Medicine, Chinese Academy of Sciences, Hangzhou 310018, China;

<sup>3</sup>School of Chemistry and Chemical Engineering, Hefei University of Technology, Hefei 230009, China;

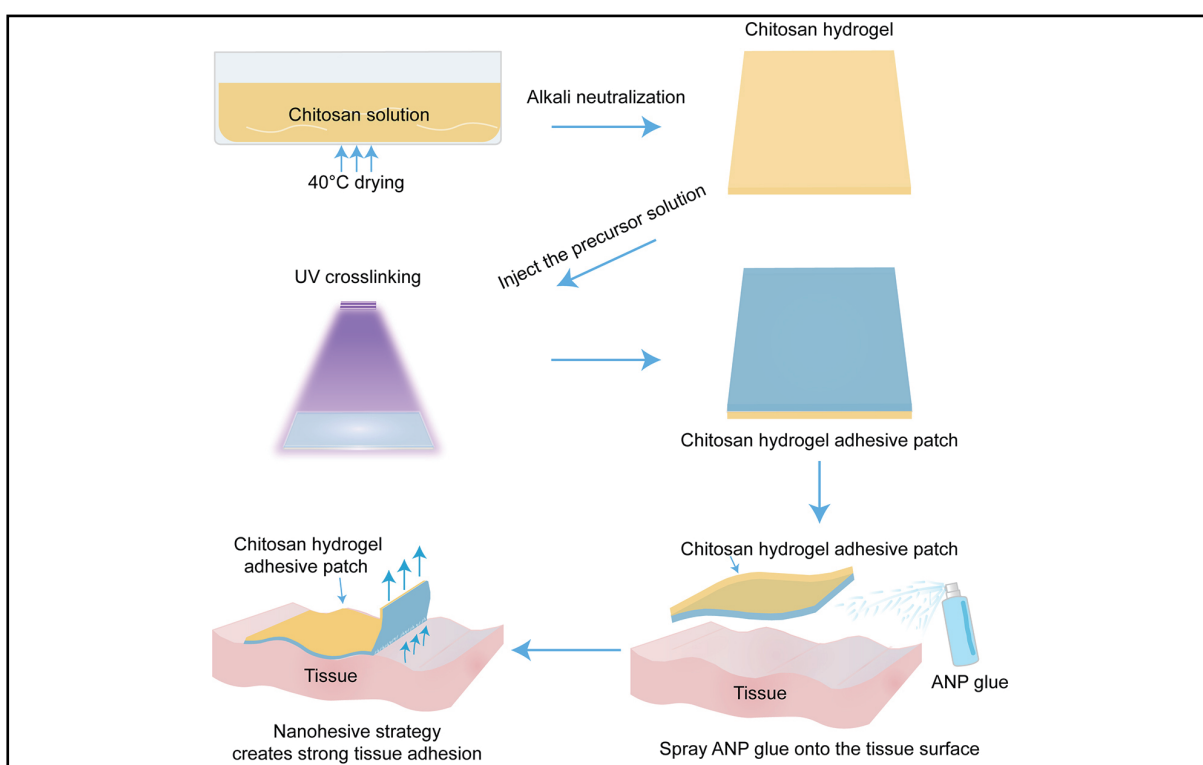
<sup>4</sup>College & Hospital of Stomatology, Anhui Medical University, Key Lab. of Oral Diseases Research of Anhui Province, Hefei 230032, China;

<sup>5</sup>Department of General Surgery, Anhui No.2 Provincial People's Hospital, Hefei 230601, China

✉Correspondence: Dong-Quan Liu, E-mail: [totoro91@foxmail.com](mailto:totoro91@foxmail.com); Liang Dong, E-mail: [dongliang@him.cas.cn](mailto:dongliang@him.cas.cn)

© 2024 The Author(s). This is an open access article under the CC BY-NC-ND 4.0 license (<http://creativecommons.org/licenses/by-nc-nd/4.0/>).

## Graphical abstract





*With the aid of a nanoadhesive strategy, a dual-layer chitosan hydrogel adhesive patch demonstrated excellent tissue wound adhesion capability.*

## Public summary

- A transparent chitosan hydrogel patch with excellent adhesion, mechanical properties, and biocompatibility was prepared.
- The tensile stress, elongation at break, toughness, maximum strength, and fracture toughness all increase with increasing thickness of the chitosan hydrogel.
- The hydrogel patch demonstrates excellent tissue wound adhesion capability.

# Highly transparent and strong nanohesive hydrogel patch for tissue adhesion

Qing Luo<sup>1,2</sup>, Zhao Pan<sup>2</sup>, Yong-Hong Song<sup>3</sup>, Jie-Yu Huang<sup>1,2</sup>, Hui Fang<sup>4</sup>, Dong-Quan Liu<sup>5</sup> , and Liang Dong<sup>2</sup> 

<sup>1</sup>College of Materials Science and Engineering, Zhejiang University of Technology, Hangzhou 310014, China;

<sup>2</sup>Zhejiang Cancer Hospital, Hangzhou Institute of Medicine, Chinese Academy of Sciences, Hangzhou 310018, China;

<sup>3</sup>School of Chemistry and Chemical Engineering, Hefei University of Technology, Hefei 230009, China;

<sup>4</sup>College & Hospital of Stomatology, Anhui Medical University, Key Lab. of Oral Diseases Research of Anhui Province, Hefei 230032, China;

<sup>5</sup>Department of General Surgery, Anhui No.2 Provincial People's Hospital, Hefei 230601, China

 Correspondence: Dong-Quan Liu, E-mail: [totoro91@foxmail.com](mailto:totoro91@foxmail.com); Liang Dong, E-mail: [dongliang@him.cas.cn](mailto:dongliang@him.cas.cn)

© 2024 The Author(s). This is an open access article under the CC BY-NC-ND 4.0 license (<http://creativecommons.org/licenses/by-nc-nd/4.0/>).



Cite This: *JUSTC*, 2024, 54(3): 0304 (11pp)



Read Online

**Abstract:** This research aimed to design and fabricate a biocompatible dual-layer chitosan hydrogel adhesive patch with exceptional mechanical properties by employing a nanoadhesive strategy to assess its tissue adhesion performance. The design involves physical cross-linking to construct a robust chitosan hydrogel as a backing membrane, followed by in situ photocuring to create the adhesive hydrogel layer, resulting in an integrated chitosan hydrogel adhesive patch. To facilitate adhesion between the hydrogel patch and biological tissue, surface-activated silica nanoparticles serve as interfacial connectors, analogous to nanoglue, promoting binding of the hydrogel to the substrate. Characterization of the patch reveals an adhesive energy of 282 J/m<sup>2</sup> to biological tissues in vitro and a burst pressure of 450 mmHg (1 mmHg=0.133 kPa). The patch exhibits outstanding mechanical properties, with a tensile strength of 4.3 MPa, an elongation rate of 65%, and a fracture toughness of 3.82 kJ/m<sup>2</sup>. Additionally, the nanoheesion-based chitosan hydrogel adhesive patch is highly transparent and demonstrates excellent biocompatibility. It holds promise for applications in various biomedical fields, including tissue repair and drug delivery, thereby providing a robust material foundation for advancements in clinical surgery.

**Keywords:** hydrogel patch; nanoheesion; chitosan; nanoglue; dual-layer structure

**CLC number:** R318.08

**Document code:** A

## 1 Introduction

Advances in tissue adhesives based on hydrogels have sparked significant interest in the field of biomedicine, leading to the development of various applications<sup>[1–3]</sup>. Hydrogel adhesives, characterized by their high water content, good biocompatibility, tissue adhesiveness, and mechanical performance, hold great potential in tissue engineering<sup>[4–6]</sup>. Homogeneous hydrogel adhesives can be readily prepared through a straightforward fabrication process, but most of them exhibit lower strength and are susceptible to rupture or detachment<sup>[7,8]</sup>. In contrast, dual-layer hydrogel adhesives offer several advantages, including superior adhesion, enhanced mechanical performance, dressing capabilities, and flexibility for independent component design<sup>[9–11]</sup>. These dual-layer hydrogel adhesives have extensive applications in biomedicine, such as postoperative adhesion prevention, bone and cartilage disease treatment, and ligament regeneration<sup>[12,13]</sup>. For instance, Peng et al.<sup>[14]</sup> proposed a novel adhesive/anti-adhesive Janus tissue patch, with one side displaying strong adhesiveness for hemostasis and the other effectively preventing postoperative tissue adhesion. Yao et al.<sup>[15]</sup> attempted to construct a new type of injectable bilayer composite hydrogel using chitosan, silk fibroin protein, hyaluronic acid,

nanoparticles and amino-functionalized mesoporous bioactive glass NPs, which exhibited multiple network structures. This hydrogel can be used in bone and cartilage tissue engineering as an injectable biomaterial for bone and cartilage repair applications. Additionally, Li et al.<sup>[16]</sup> developed a mussel-inspired adhesive bilayer hydrogel based on silver nanoparticles. The top layer is composed of carboxymethyl chitosan with antibacterial activity to prevent infection. In contrast, the bottom layer, made of polyvinyl alcohol (PVA) and polyethylene glycol (PEG) as foaming agents, absorbs wound exudate and facilitates oxygen exchange. Silver nanoparticles impart antibacterial properties to bilayer hydrogels, promoting the healing process. In summary, dual-layer hydrogel adhesives can combine the properties mentioned above due to their unique structure and various preparation methods.

In this study, we propose a fabrication strategy to obtain a chitosan hydrogel adhesive patch with a dual-layer structure in which the two layers have different compositions and functions. The resulting membrane consists of chitosan hydrogel, a natural polymer known for its biocompatibility, antibacterial activity, and biodegradability, which is widely used in the biomedical field<sup>[17–19]</sup>. The adhesive layer is formed by coating a certain thickness of precursor solution on the surface of a chitosan hydrogel and inducing polymerization through



ultraviolet (UV) exposure. The precursor solution comprises *N,N*-dimethylacrylamide (DMA), a photoinitiator, a cross-linking agent, and a gelatin aqueous solution. Poly *N,N*-dimethylacetamide (PDMA) has advantages, including biocompatibility, water solubility, flexibility, elasticity, and excellent water-absorption capacity, and it holds significant promise in medical and biomaterials applications<sup>[20–22]</sup>. Gelatin is recognized for its good biocompatibility, minimal ability to cause immune reactions, and it is commonly used in medicine and biomaterials<sup>[23–25]</sup>. To establish the bonding between the hydrogel patch and substrate, nanoglue was introduced, with nanoparticles serving as interfacial connectors, which bind the hydrogel to biological tissues, following our previous research<sup>[26]</sup>. The adhesive performance, mechanical properties, transparency, microstructure, and biocompatibility of the dual-layer chitosan hydrogel adhesive patch were investigated. The exploration of tissue adhesion through chitosan hydrogel adhesive patches is highly important for the extensive utilization of adhesive patches across various biomedical domains, including tissue repair and drug delivery. These findings establish a robust material foundation for advancements in clinical surgical medicine.

## 2 Materials and methods

### 2.1 Materials and instruments

Chitosan (CS, high viscosity), acetic acid, ammonium hydroxide, and anhydrous ethanol were purchased from China National Pharmaceutical Group Chemical Reagent Co., Ltd.; 3-aminopropyltriethoxysilane (APTES), succinic anhydride (SA), 4-dimethylaminopyridine (DMAP), *N,N*-dimethylformamide (DMF), *N,N*-dimethylacrylamide (DMA), gelatin, *N,N'*-bis(acrylamide)cystamine (BAC), and I-1173 were purchased from Shanghai Aladdin Company. MEM (Gibco, USA), phosphate-buffered saline (PBS) (Gibco, USA), fetal bovine serum (Gibco, USA), pancreatic enzyme cell digestion solution (0.25% trypsin, Gibco, USA), streptomycin (Gibco, USA), a CCK-8 assay kit (Dojindo Laboratories Inc., Kumamoto, Japan), and a calcein-AM/PI live/dead cell double staining reagent kit (Dojindo Laboratories Inc., Kumamoto, Japan) were used as received.

An electronic balance (BCE224-1CCN, Sartorius Scientific Instruments Co., Ltd.), a thermostatic magnetic stirrer (S10-3, Shanghai Sile Instruments), a mechanical stirrer (RW20 digital, IKA, Germany), a centrifuge (Thermo Fisher), a heating platform (X4060, Shenzhen Xinhao Electronic Technology), a vacuum ultraviolet lamp, a universal material testing machine (KZ-DSC-500, Suzhou Kezhun Measurement and Control), an ultrasonic cell disruptor (SCIENTZ-IIID, Ningbo Xinzhi Biological Technology), a heat-collecting constant-temperature magnetic stirrer (DF-101S, Shanghai Lichenbangxi Instrument Technology), a field emission scanning electron microscope (JSM-IT800, JEOL, Japan), a sputter coater (JEC-3000FC, JEOL, Japan), and a UV/visible/near-infrared spectrophotometer (PerkinElmer LAMBDA1050+, PerkinElmer Inc., USA) were used. A high-temperature and high-pressure sterilizer (Bingshan Songyang Biological Technology), microplate reader (Biotek, USA), inverted fluorescence microscope (IX71, Olympus, Japan), and cell culture incubator (Thermo Scientific, USA) were used.

### 2.2 Synthesis

#### 2.2.1 Preparation of hydrogel patches

**Hydrogel patch backing preparation.** Six grams of chitosan powder was weighed and added to a 288 mL beaker containing deionized water. The powders were suspended using mechanical stirring. Then, 6 mL of acetic acid was gradually added while stirring, and stirring was continued until the solution became clear and transparent. The solution was centrifuged for 20 min, and then vacuum extraction was performed to remove bubbles. Next, the solution was poured into a 100 mm×100 mm square dish, and 25 mL (25CS), 50 mL (50CS), or 75 mL (75CS) of solution was added. It was dried at 40 °C to form a film. After the film had completely dried, it was removed and soaked in an ammonium hydroxide solution for 4 h. The chitosan hydrogel was removed, and any residual solution on the surface was rinsed off with deionized water. Finally, it was stored in deionized water for later use.

**Preparation of surface-activated nanoparticle (ANP)-based glue (ANP glue).** In brief, silica nanoparticles (1 g) were fully dispersed in ethanol (1 L) through ultrasonication and gentle stirring for 0.5 h. Subsequently, a DMF solution (10 mL) containing APTES (1 mol/L), succinic anhydride (1 mol/L), and DMAP (0.01 mol/L) was added to the dispersed nanoparticles, and the mixture was maintained at 60 °C under magnetic stirring for 12 h. The entire solution was collected by centrifugation, and the nanoparticles were washed several times with ethanol to remove residual reactants. Afterward, they were dried, crushed into powder, and stored. When needed, the powder was reconstituted in a 20% solution.

**Preparation of the hydrogel patch precursor solution.** To prepare a 2% gelatin solution, 0.2 g of gelatin was weighed and combined with 9.8 g of deionized water in an amber vial, which was then placed in a light-protected environment. The mixture was heated and stirred in a 60 °C water bath until complete dissolution. Subsequently, 3.46 g of DMA, a small amount of BAC, and photosensitizer I-1173 were added. The solution was stirred thoroughly at room temperature. Gelatin solutions with concentrations of 0%, 1%, 2%, and 3% were prepared depending on the gelatin content.

The prepared chitosan hydrogel was placed onto a preprepared template. The chitosan hydrogel was secured onto the template using 3M tape, and the precursor solution was evenly dripped onto the surface of the chitosan hydrogel. Under nitrogen protection, the sample was positioned under a 365 nm ultraviolet lamp for a cross-linking reaction for a duration of 1 h. Following the cross-linking reaction, the desired chitosan hydrogel adhesive patch was obtained. The chitosan hydrogel adhesive patch with a 25CS backing film is called the 25C-PDMA adhesive patch.

#### 2.2.2 Evaluation and presentation of the adhesive properties of the hydrogel patch

To demonstrate the adhesive properties of the chitosan hydrogel adhesive patch, we primarily conducted adhesion experiments on the porcine liver and porcine heart to observe the entire adhesion process. Additionally, we used a 180° peeling test and burst tests to evaluate the performance of chitosan

hydrogel adhesive patches with different backing membrane thicknesses in bonding porcine skin and collagen casings.

The 180° peeling test protocol involved constructing an adhesive interface using porcine skin and a collagen casing as the adherent substrates to obtain the required test samples. The bonded area of the 180° peeling test samples was 10 mm × 60 mm. One hundred microliters of ANP glue was sprayed onto the adherent interface, and a 500 g weight was placed vertically on the bonding device to provide pressure. After recording the sample width ( $W$ ), the tests were conducted on a mechanical testing machine at a pulling speed of 100 mm/min to measure the maximum load ( $F$ ) for each sample, according to formula (1).

$$\text{Interface toughness (J/m}^2\text{)} = 2F/W. \quad (1)$$

In this context, the unit for the maximum load is in Newtons (N), and the unit for width is in meters (m).

The main process of the burst pressure test is that during injection, a continuous infusion of PBS solution through 2 mm holes in the collagen casing was maintained to impact the chitosan hydrogel adhesive patch until the barrier was breached. This method was employed to measure the maximum pressure that the material could withstand during blood outflow. The chitosan hydrogel adhesive patch samples used in the experiment were square with dimensions of 10 mm × 10 mm, were coated with 30  $\mu$ L of ANP glue on their surfaces, and were constructed alongside moistened collagen casing to form the adhesive interface. An injection pump was used to infuse PBS solution at a rate of 20 mL/min while recording the state of each sample at the time of failure and the reading on the pressure gauge. The detachment of the hydrogel matrix was regarded as the criterion for failure of the chitosan hydrogel adhesive patch. For subsequent statistical analysis, the pressure gauge reading was multiplied by 7.5 to convert the pressure values to units of millimeters of mercury.

### 2.2.3 Characterization of the hydrogel patch

The evaluation of the mechanical properties of the CS hydrogel and chitosan hydrogel adhesive patch was primarily conducted through a tensile test. We employed a universal mechanical testing machine for this purpose. First, the chitosan hydrogel adhesive patches were cut into dumbbell-shaped samples with a central length of 10 mm and width of 2 mm using a dumbbell-shaped cutter. During testing, a tensile speed of 100 mm/min was used, and the tensile stress, tensile strain, and load data were recorded. To test the fracture toughness of the chitosan hydrogel adhesive patches, samples were cut to dimensions of 2 cm in length and 1 cm in width. These patches were affixed to PMMA plates using Loctite 403 glue, with approximately 5 mm of sample width left for testing. For samples with notches, an artificial notch was created, measuring one-fourth to one-half of the length. By conducting notched tests, we determined the strain at which the sample had fractured. The mechanical test was performed in deionized water.

**Swelling ratio testing.** Chitosan hydrogel samples of different thicknesses were prepared into circular discs with a diameter of 10 mm. These discs were then dried in a 60 °C oven for 2 d. The samples were immersed in PBS, and at regular intervals, the gel samples were removed, and any water

droplets on the surface were removed using filter paper. The gels were weighed precisely until their weight remained substantially stable without further changes. The swelling ratio was calculated using the following formula (2):

$$\text{Swelling rate(\%)} = (W_{\text{after}} - W_{\text{initial}}) / W_{\text{initial}} \times 100\%, \quad (2)$$

where  $W_{\text{initial}}$  and  $W_{\text{after}}$  represent the weights before and after swelling, respectively.

Additionally, for hydrogel patches with different thicknesses, we utilized a UV-Vis spectrophotometer for transparency testing in the range of 250–800 nm. The target hydrogels were dried in an oven and then subjected to cryo-fracture treatment using liquid nitrogen, followed by gold sputter coating. Finally, we employed scanning electron microscopy (SEM) to capture the microscopic morphology of the hydrogel interface, enabling further observation of its structure and characteristics. For TEM analysis, 0.25 g of prepared ANP powder was dissolved in 4.75 g of anhydrous ethanol. The solution was sonicated for 10 min, and then 10  $\mu$ L of the solution was dropped onto a copper grid for TEM observation. For DLS analysis, 0.5 g of prepared ANP powder was dissolved in 9.5 g of deionized water. The solution was sonicated for 10 min.

### 2.2.4 Assessment of the biocompatibility of the hydrogel patch

The sample preparation for the experiment was conducted as follows: CS and C-PDMA were obtained and dissolved in physiological saline solution to prepare the material extraction solution at a concentration of 20 mg/mL. Five milliliters of anticoagulated pig blood was centrifuged at 4500 r/min for 15 min to remove the supernatant. The red blood cells were gently washed three times with physiological saline solution in a centrifuge tube, followed by centrifugation at 4500 r/min for 15 min after each wash. After the washing steps, the red blood cells were diluted with physiological saline solution to a final concentration of 5% (v/v) to prepare the red blood cell suspension. Five milliliters of the material extraction solution, physiological saline solution, and deionized water were added to the prepared red blood cell suspension (physiological saline solution and deionized water served as the negative and positive control groups, respectively). The mixture was incubated at 37 °C for 1 h. Subsequently, the red blood cell suspension was centrifuged at 4500 r/min for 15 min, and images were captured. Finally, the OD (optical density) values at 540 nm were measured using an enzyme-linked immunosorbent assay reader, and the hemolysis rate was calculated according to the following formula (3):

$$\text{Hemolysis rate(\%)} = (\text{OD}_{\text{sample}} - \text{OD}_{\text{negative}}) / (\text{OD}_{\text{positive}} - \text{OD}_{\text{negative}}) \times 100\%, \quad (3)$$

where  $\text{OD}_{\text{sample}}$ ,  $\text{OD}_{\text{negative}}$ , and  $\text{OD}_{\text{positive}}$  represent the OD values of the experimental group, negative control group, and positive control group, respectively. According to ISO 10993-4 and the relevant literature<sup>[27]</sup>, the national standard requires a hemolysis rate not exceeding 5%. A hemolysis rate exceeding this threshold indicates that the material exhibits hemolytic activity.

To evaluate the in vitro biocompatibility, the CS hydrogel

was used as the control group, and the 25C-PDMA adhesive patches were used as the experimental group. Both groups underwent high-temperature and high-pressure sterilization. Subsequently, they were immersed in complete DMEM culture medium containing 10% FBS and 1% dual antibodies at a ratio of 1 g/10 mL. The samples were then incubated in a cell culture incubator at 37 °C with 5% CO<sub>2</sub> for 24 h to facilitate extraction.

L929 mouse fibroblasts were seeded in 96-well plates at a density of 3×10<sup>3</sup> cells per well. The plates were placed in a cell culture incubator at 37 °C with 5% CO<sub>2</sub> for 24 h. The cells were cultured for 1, 4, and 7 d. At the end of each designated culture period, CCK-8 reagent was mixed with pure DMEM at a 1 : 9 ratio. The mixture was added to each well and incubated for 2 h. The OD of each well was measured at a wavelength of 450 nm using a microplate reader.

For cell viability staining, a staining solution was prepared by mixing 10 μL of calcein AM and 15 μL of PI in 5 mL of PBS. L929 mouse fibroblasts were incubated with the staining solution for 30 min. After incubation, the cells were washed and observed under an upright fluorescence microscope to determine the conditions of live and dead cells.

To evaluate the *in vivo* biocompatibility, a rat subcutaneous inflammation model was constructed. The surgical protocol for subcutaneous implantation experiments in rats was reviewed and approved by the Animal Ethics Committee of the Institute of Basic Medical Sciences and Cancer Research, Chinese Academy of Sciences (2023R-0081). All the experimental procedures strictly complied with the Laboratory Animal Care and Use Guidelines. Male SD rats (7–8 weeks old) free of pathogenic bacteria were used for *in vivo* biocompatibility studies. The selected experimental animals were randomized, the blinding method was not used, nor were the exclusion criteria included. All experimental animals were housed in well-ventilated animal rooms, provided with sterile food and water, and maintained on a 12-h light/dark cycle.

During the surgical procedure, the rats were first anesthetized with isoflurane. The hair in the surgical area on the back was shaved, and the area was disinfected with iodine. Subsequently, two points on either side of the midline of the back were selected. The skin was incised to separate the subcutaneous tissue, exposing the back muscles of the rats. Then, the prepared sterile materials were implanted and fixed subcutaneously according to the grouping. Finally, the incision was sutured with surgical thread. One and two weeks after surgery, the rats were euthanized painlessly. The implanted tissues were excised and fixed with 4% paraformaldehyde for more than 24 h. Then, the samples were embedded in paraffin, sectioned, and stained with HE and Masson's trichrome. The sections were observed using a biological microscope. These studies focused mainly on the appearance and degree of fibrosis and inflammation in the implanted tissue.

Overall, these experiments were conducted to assess the *in vitro* biocompatibility of the CS hydrogel (25CS) and 25C-PDMA adhesive patches.

For the statistical analysis, the independent *t* test was used to compare continuous variables between two groups, while one-way analysis of variance (ANOVA) was used to assess differences among three or more groups. Statistical analyses

were conducted using GraphPad Prism 9.5. The notation “ns” indicates nonsignificant differences, while “\*, *P* < 0.05,” “\*\*\*, *P* ≤ 0.01,” and “\*\*\*\*, *P* ≤ 0.001” indicate statistical significance at the corresponding level.

## 3 Results and discussion

### 3.1 Hydrogel patch preparation process and morphology

On the surface of the chitosan hydrogel, a precursor solution was uniformly coated, and under nitrogen protection, 365 nm ultraviolet irradiation was applied to induce the polymerization of well-dispersed DMA in the presence of Irgacure I-1173 and the crosslinking agent BAC, resulting in the formation of a cationic PDMA hydrogel. The synthesis and utilization process of the nanohectic-based chitosan hydrogel adhesive patch is visually represented in Fig. 1a. This hydrogel, interpenetrated with a thermoresponsive gelatin network from the precursor solution, forms a dual-network hydrogel layer. When the precursor solution is placed on the chitosan hydrogel surface, the chitosan hydrogel exhibits excellent permeability and a mesh-like structure, allowing solute molecules in the precursor solution to freely diffuse within the gel. Consequently, the chitosan hydrogel tightly bonds with the newly formed dual-network hydrogel layer, creating an integrated bilayer hydrogel patch. Fig. 1b, c, d, e shows the chitosan hydrogel sample, the UV crosslinking diagram, the chitosan hydrogel adhesive patch sample, and the porcine muscle adhesion display, respectively.

### 3.2 Characterization of the properties of ANP and chitosan hydrogels

For nanohectic ANP, we believe that this is the main reason for adhesive formation, and the mechanism of nanohectic involves interfacial adsorption and interaction processes. In this design, the viscous hydrogel layer can rapidly absorb the interfacial water layer of the adhesive and tissue surface, thereby promoting close contact between the adhesive layer and the tissue. In the ANP adhesive, a large number of nanoparticle aggregates are dispersed, which increases the dehydration density and further promotes close contact between the adhesive layer and the substrate.

First, we characterized the morphology of the nanoparticles using transmission electron microscopy (TEM), as shown in Fig. 2a, revealing the particle size distribution trend. The corresponding hydration radius of these nanoparticles was determined by dynamic light scattering (DLS) measurements, and the statistical distribution is presented in Fig. 2b, with an average nanoparticle size of 69.9 nm. The zeta potential of the nanoparticles was also measured, as shown in Fig. 2c, with a value of −32.5 mV, indicating a negative charge.

Different thicknesses of the same type of hydrogel may exhibit variations in their stress–strain curves when subjected to tensile loading. To investigate this phenomenon, we conducted mechanical tensile tests on hydrogels with different thicknesses of chitosan. Fig. 2d shows the stress–strain curves of the chitosan hydrogels, revealing that thinner hydrogels generate more stress. Fig. 2e presents the statistical results of the mechanical strength of the chitosan hydrogels with varying



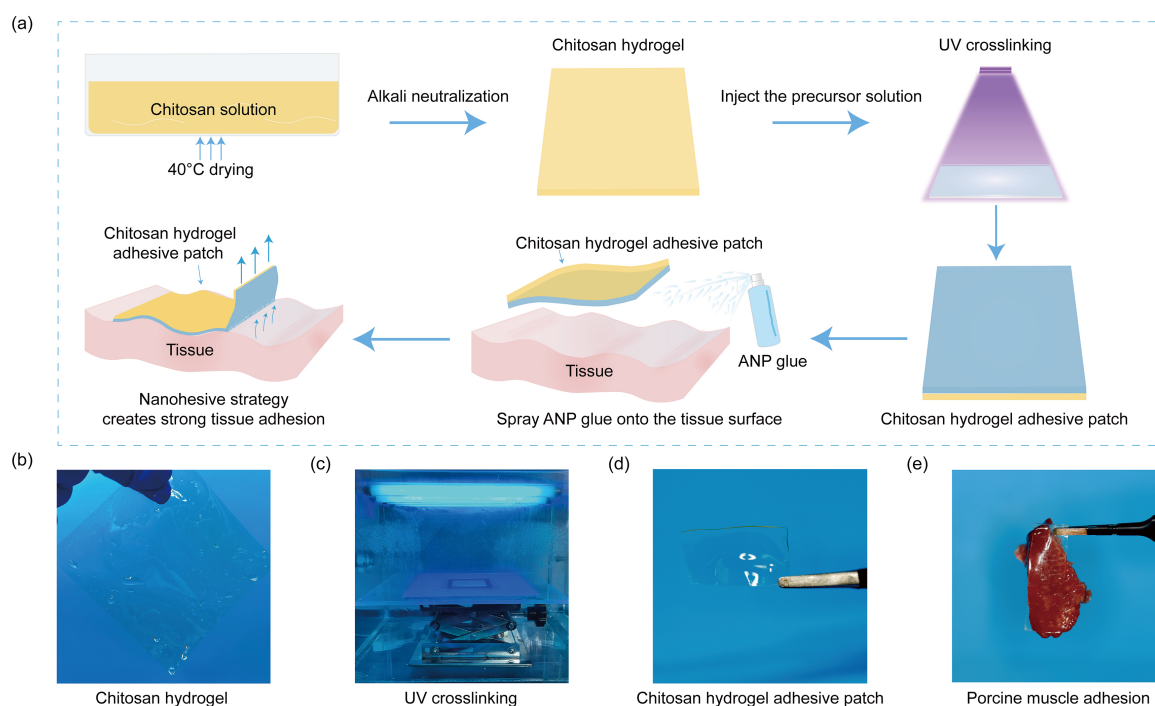


**Fig. 1.** Design and fabrication of chitosan hydrogel adhesive patches. (a) Schematic of the fabrication and application process for nanohesion-based chitosan hydrogel adhesive patches. (b) Chitosan hydrogel sample. (c) Ultraviolet crosslinking. (d) Sample of chitosan hydrogel adhesive patch. (e) Demonstration of nanohesion to porcine muscle by a chitosan hydrogel adhesive patch.

thicknesses, indicating a decreasing trend in the mechanical strength with increasing thickness. Fig. 2f displays the variation in fracture elongation, with the 50CS group exhibiting the highest average fracture elongation of 197.6%. By integrating the stress–strain curves of chitosan hydrogels with different thicknesses, we obtained their toughness, as shown in Fig. 2g. Additionally, Fig. 2i reveals the swelling ratio, with the 50CS group exhibiting a slightly greater swelling ratio than the other two groups. This suggests that the water content within chitosan hydrogels may also influence their toughness. Specifically, the average toughness of the 25CS group reached 24.2 kJ/m<sup>2</sup>, that of the 50CS group reached 28.4 kJ/m<sup>2</sup>, and that of the 75CS group reached an average toughness of 22.7 kJ/m<sup>2</sup>. Finally, Fig. 2h presents the Young's modulus of the hydrogels, indicating no significant difference in the average Young's modulus among the three groups.

### 3.3 Assessment of the adhesive properties of the hydrogel patches

The adhesive performance of the chitosan hydrogel adhesive patch was investigated using fresh ex vivo porcine liver and porcine heart tissue specimens. As shown in Fig. 3a, b, a distinct wound area was carefully created on the fresh porcine liver and porcine heart tissues using a surgical scalpel. ANP glue was uniformly applied to the wound surface, followed by immediate application of the chitosan hydrogel adhesive patch to the wound area. This resulted in the effective closure of the wound through the adhesive action of the chitosan hydrogel adhesive patch, which acted as an effective physical sealant and demonstrated durable adherence to the biological tissues.

To assess the adhesive capabilities of the chitosan hydrogel adhesive patch, a 180° peeling test and burst pressure test were conducted using fresh ex vivo porcine skin and moistened synthetic collagen casing as testing substrates. Fig. 3c provides a schematic representation of the 180° peeling test and burst pressure test.

Polyethylene terephthalate (PET) is utilized as the backing membrane to mitigate excessive deformations of the soft hydrogel layer, thus ensuring the implementation of a more standardized testing procedure. A 180° peeling test was conducted using fresh porcine skin as the adhesive substrate to evaluate the influence of the gelatin content in the second network of the dual-network hydrogel on the interfacial toughness. The findings revealed that an increase in the gelatin content led to an initial increase followed by a subsequent decrease in the interfacial toughness of the adhesive patch when PET was used as the backing membrane. Specifically, the average interfacial toughness increases from 138.2 J/m<sup>2</sup> to 280.9 J/m<sup>2</sup>. However, when the gelatin content reached 3%, the average interfacial toughness decreased to 56.7 J/m<sup>2</sup> (Fig. 3d).

In a dual-network structure, the augmentation of the gelatin content, which serves as the second network, leads to a higher polymer chain density within the gelatin network, thereby enhancing the stability of the dual-network hydrogel. Furthermore, the increased concentration of gelatin led to increased intermolecular cross-linking between the gelatin molecules, resulting in the formation of a denser network structure. In contrast, the density of the PDMA polymer chains in the first network decreases. Before applying the adhesive, ANP glue was sprayed onto the substrate surface. When the gelatin content is excessively increased, the proportion of

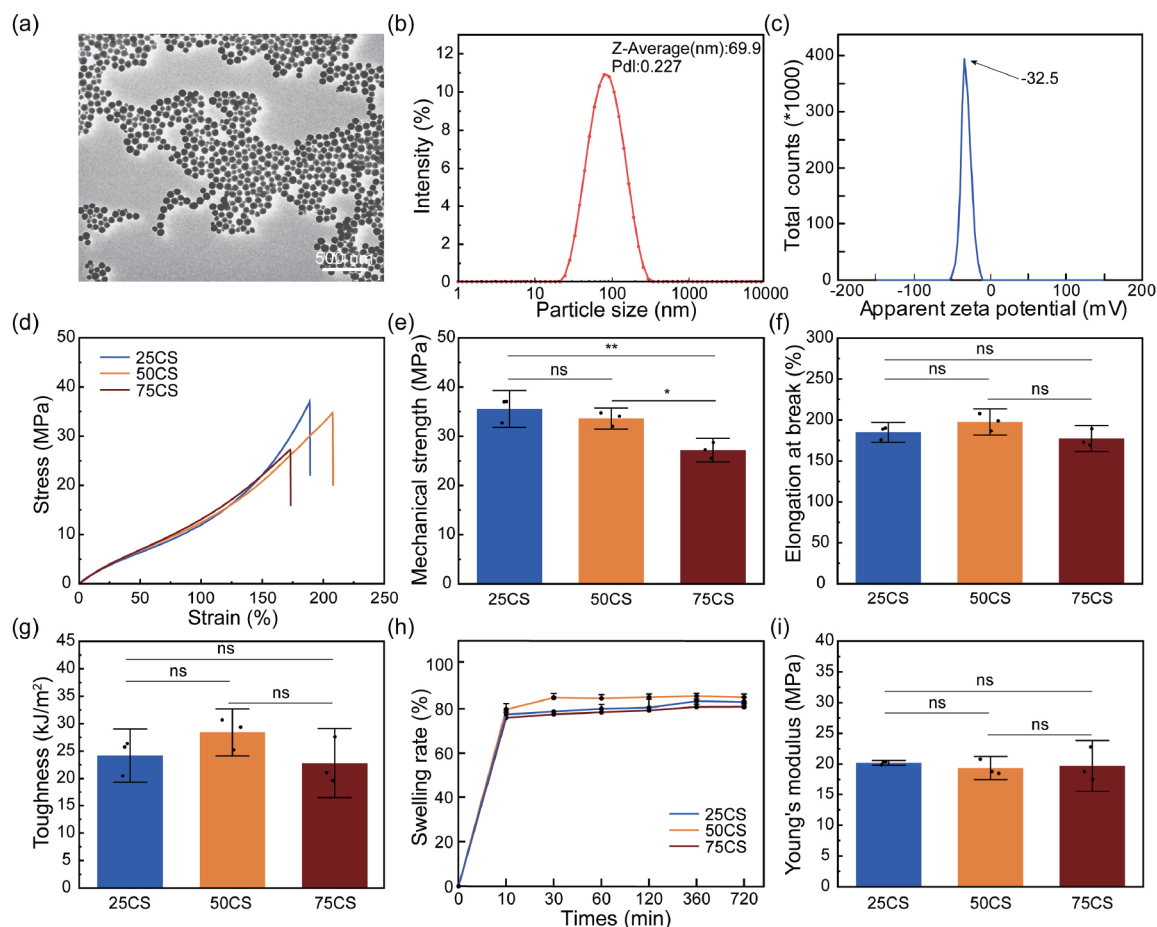


**Fig. 2.** Characterization of ANP and chitosan hydrogel. (a) TEM image of ANP. (b) The distribution of hydrodynamic sizes of ANP measured by DLS. (c) Zeta potential of ANP. (d) Stress-strain diagram of the chitosan hydrogel. (e) Maximum tensile stress of the chitosan hydrogel. (f) Elongation at break of the chitosan hydrogel. (g) The toughness of the chitosan hydrogel. (h) Swelling rate of the chitosan hydrogel. (i) Young's modulus of the chitosan hydrogel. The values represent the means  $\pm$  SDs ( $n = 3$ ). The statistical significance was determined using one-way ANOVA; ns, not significant; \*,  $P < 0.05$ ; \*\*,  $P \leq 0.01$ .

PDMA decreases correspondingly, affecting the binding between the ANP glue and PDMA molecular chains and reducing the number of adhesive sites. The optimum adhesive effect was observed when the gelatin content was 2%.

With a 2% gelatin content, we conducted 180° peeling tests on chitosan hydrogel adhesive patches with varying backing membrane thicknesses. Compared with that of porcine skin, the interfacial toughness is generally greater when a synthetic collagen casing is used as the adherent substrate. For instance, when porcine skin served as the adherent substrate, the average interfacial toughness of the 25C-PDMA adhesive patch was measured to be 205.3 J/m<sup>2</sup>. However, when a synthetic collagen casing was used as the adherent substrate, it increased to 282.1 J/m<sup>2</sup>. Similarly, for the 75C-PDMA adhesive patch, the average interfacial toughness decreased from 70.2 J/m<sup>2</sup> on porcine skin to 133 J/m<sup>2</sup> on the synthetic collagen casing as the backing material (Fig. 3e). The observed difference in interfacial toughness can be attributed to the influence of surface characteristics. As the adhesive patch thickness increases, the susceptibility to surface irregularities or discrepancies in microstructures increases. Consequently, the capacity for deformation within the adhesive layer decreases, making it less adaptable to conform to the adhering

surface. This reduction in flexibility diminishes the effective contact area for adhesion and ultimately leads to a decrease in adhesive strength. In summary, the choice of adherent substrates, such as synthetic collagen casings or porcine skin, significantly affects the interfacial toughness of chitosan hydrogel adhesive patches. The increasing thickness of the adhesive patch can compromise its ability to conform to surface irregularities, resulting in reduced adhesive strength.

A burst pressure test was conducted using a collagen casing as the adherent substrate. During the testing, it was observed that the maximum burst pressure of the chitosan hydrogel adhesive patch resulted in the leakage of the PBS solution from the edges of the bonding interface. However, this leakage did not compromise the structural integrity of the chitosan hydrogel adhesive patch, indicating the effective protection of the adhesive layer by these chitosan hydrogel adhesive patches of varying thicknesses. The average burst pressures for the 25C-PDMA, 50C-PDMA, and 75C-PDMA adhesive patches were 451.4 mmHg (1 mmHg=0.133 kPa), 310 mmHg, and 263.1 mmHg, respectively. These values all exceeded the normal human blood pressure of 220 mmHg (Fig. 3f). Furthermore, as the thickness increased, the ability to withstand burst pressure decreased. Thickness also



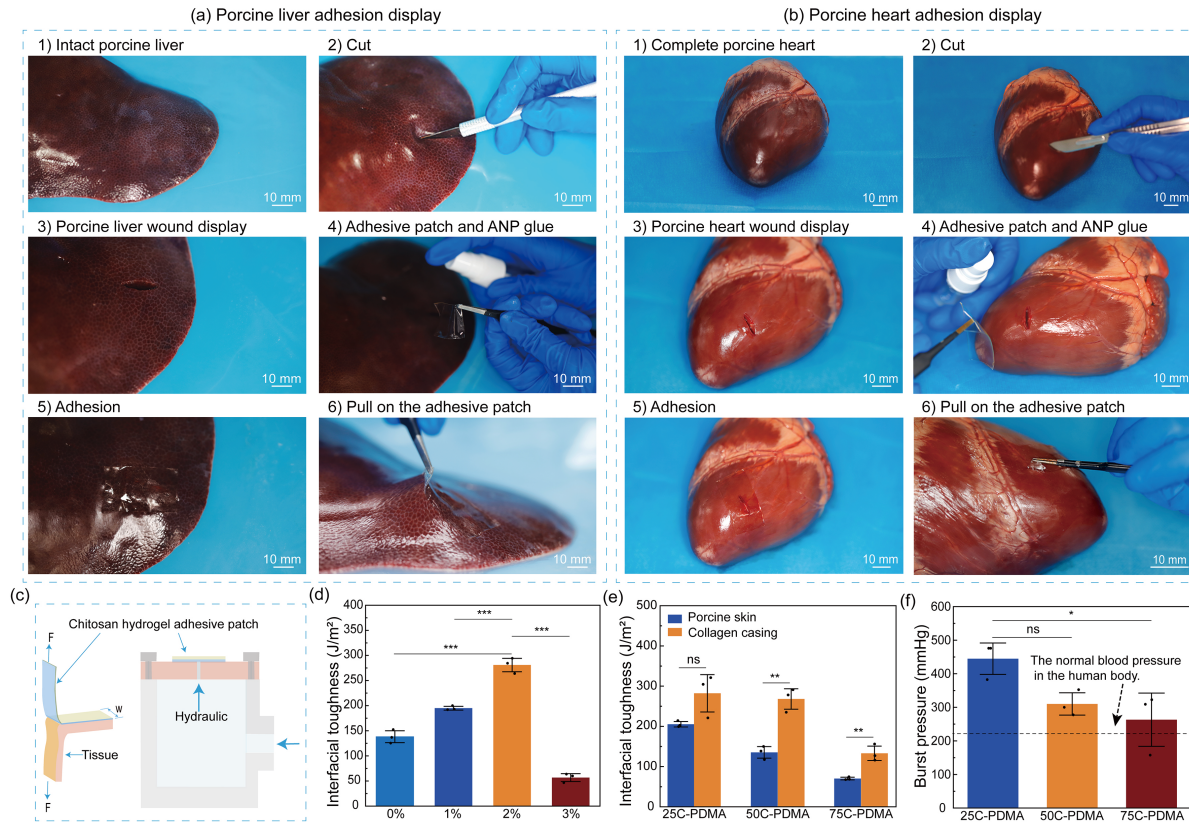


**Fig. 3.** Characterization of the adhesive properties of the chitosan hydrogel adhesive patch. (a) Adhesion of the chitosan hydrogel adhesive patch to porcine liver tissue. (b) Adhesion of the chitosan hydrogel adhesive patch to porcine heart tissue. (c) Schematic illustration of the 180° peeling test and burst pressure test. (d) Interfacial toughness of the adhesive layer at different gelatin contents. (e) Interfacial toughness of chitosan hydrogel adhesive patches with different thicknesses on various adherent substrates. (f) Burst pressure tolerance of chitosan hydrogel adhesive patches with different thicknesses. The values represent the means  $\pm$  SDs ( $n = 3$ ). The statistical significance was determined using the  $t$  test and one-way ANOVA; ns, not significant; \*,  $P < 0.05$ ; \*\*,  $P \leq 0.01$ ; \*\*\*,  $P \leq 0.001$ .

influenced the flexibility and adaptability of the adhesive patches. Thinner adhesive patches with thinner chitosan backing membranes exhibited greater flexibility and adaptability, enabling them to conform better to materials with different shapes and surfaces. In contrast, owing to their thicker chitosan hydrogel backing, thicker adhesive patches were generally stiffer and less adaptable, potentially limiting their ability to fully conform to irregular surfaces.

### 3.4 Investigation of the mechanical properties of the hydrogel patch

The chitosan hydrogel is the primary factor influencing the mechanical performance, with the mechanical properties of the adhesive patches increasing as the thickness of the chitosan hydrogel layer increases. Fig. 4a presents stress-strain curves for adhesive patches with different thicknesses of chitosan hydrogel, while Fig. 4b displays the maximum mechanical stress for these patches. For the 25C-PDMA adhesive patch, the average stress is 4.3 MPa; for the 50C-PDMA adhesive patch, it is 8.6 MPa; and for the 75C-PDMA adhesive patch, it is 10.9 MPa. Thicker adhesive patches generally exhibit greater strength. Thicker adhesive patches contain a greater quantity of chitosan molecules, allowing them to withstand higher external pressure without rupturing. Conversely, thinner adhesive patches have fewer chitosan molecules, resulting in lower strength and increased

susceptibility to external pressure-induced fracture.

The average elongation at break for the 25C-PDMA adhesive patches was 65%, that for the 50C-PDMA adhesive patches was 105%, and that for the 75C-PDMA adhesive patches was 123% (Fig. 4c). The elongation at break of hydrogels increases with increasing thickness. This is because increased material thickness provides more mass and molecular chains of chitosan, thereby enhancing the tensile strength and ductility of the material. When a hydrogel experiences tensile stress, the internal molecular chains gradually extend until reaching the breaking point. A greater material thickness provides more molecular chains, enabling the material to withstand greater tensile forces, thereby elongating the breaking point. Thus, increasing the thickness enhances the breakage of hydrogels.

Even with different thicknesses, the same material exhibits minimal variation in Young's modulus (Fig. 4d). Fig. 4e displays the toughness of the adhesive patches with varying chitosan hydrogel thicknesses. The average toughness of the 25C-PDMA adhesive patches is 1.9 kJ/m², that of the 50C-PDMA adhesive patches is 5.6 kJ/m², and that of the 75C-PDMA adhesive patches is 8.3 kJ/m². Fig. 4f shows the load profiles for these adhesive patches. The average load for the 25C-PDMA adhesive patches is 2.7 N, that for the 50C-PDMA adhesive patches is 6.6 N, and that for the 75C-PDMA adhesive patches is 11.1 N. Fig. 4g provides a

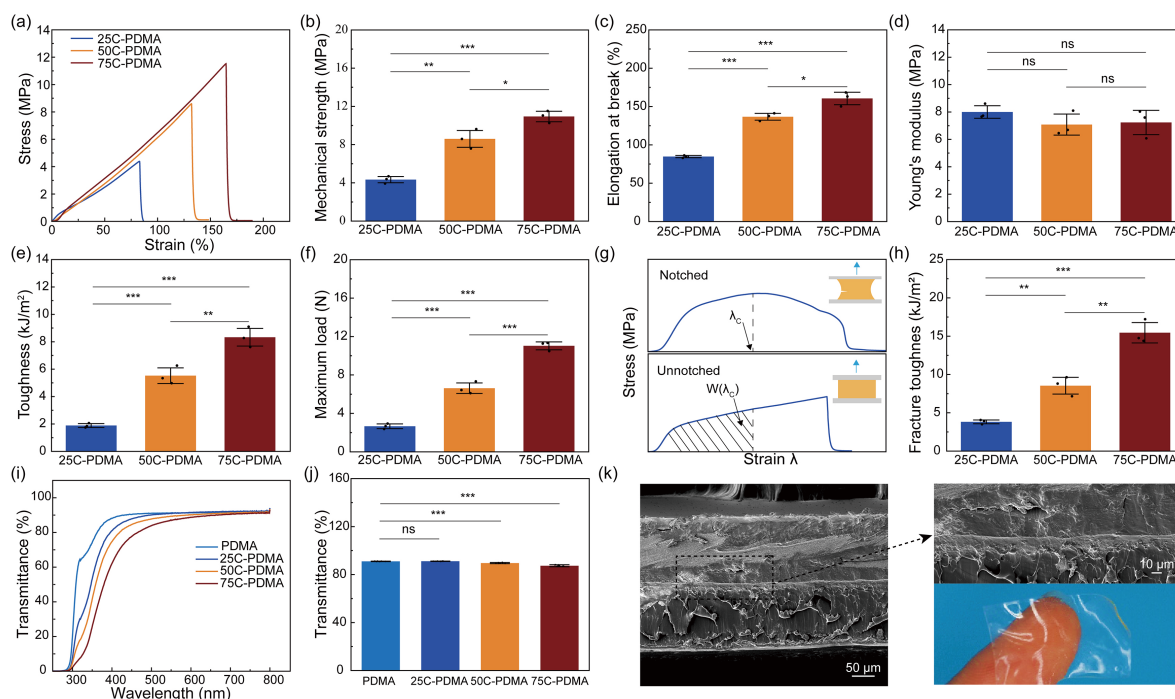


**Fig. 4.** Mechanical properties of the chitosan hydrogel adhesive patch. (a) Stress–strain diagram of the chitosan hydrogel adhesive patch. (b) Maximum tensile stress of the chitosan hydrogel adhesive patch. (c) Elongation at break of the chitosan hydrogel adhesive patch. (d) Young's modulus of the chitosan hydrogel adhesive patch. (e) Toughness of the chitosan hydrogel adhesive patch. (f) Maximum load of the chitosan hydrogel adhesive patch. (g) Diagram of a method used to measure and calculate the work of fracture and fracture toughness. (h) Fracture toughness of the chitosan hydrogel adhesive patch. (i) Transmittance of the chitosan hydrogel adhesive patch. (j) Transmittance of the chitosan hydrogel adhesive patch at 550 nm ( $n=9$ ). (k) Microstructure of the chitosan hydrogel adhesive patch and a picture of the real product. The values represent the means  $\pm$  SDs ( $n=3$ ). The statistical significance was determined using one-way ANOVA; ns, not significant; \*,  $P < 0.05$ ; \*\*,  $P \leq 0.01$ ; \*\*\*,  $P \leq 0.001$ .

schematic representation of the fracture toughness, illustrating samples with and without notches. Fig. 4h shows the fracture toughness of adhesive patches with different chitosan hydrogel thicknesses. The average fracture toughness of the 25C-PDMA adhesive patches is 3.8 kJ/m<sup>2</sup>, that of the 50C-PDMA adhesive patches is 8.5 kJ/m<sup>2</sup>, and that of the 75C-PDMA adhesive patches is 15.5 kJ/m<sup>2</sup>. A higher fracture toughness of adhesive hydrogels indicates better resistance to fracturing and the capacity to absorb more energy. This implies that hydrogels can elongate and deform without easily rupturing when subjected to external loads. Improved fracture toughness in hydrogels enhances material reliability and durability, extending their operational lifespan.

Transparency tests were subsequently conducted for chitosan hydrogel adhesive patches with different chitosan hydrogel thicknesses. Fig. 4i shows the transmittance curves obtained using a UV–visible spectrophotometer in the wavelength range of 250–800 nm. Below 290 nm, absorption peaks are nearly absent, and the transmittance is extremely low. As the wavelength increased, the transmittance of the chitosan hydrogel adhesive patch significantly increased, reaching nearly 94%. Fig. 4j provides statistics on the transmittance at 550 nm for each chitosan hydrogel adhesive patch. Chitosan hydrogel adhesive patches without a backing film exhibited an average transmittance of 91.01%, while 25C-PDMA adhesive patches had an average transmittance of 90.08%, 50C-PDMA adhesive patches had an average transmittance of 89.56%, and 75C-PDMA adhesive patches had an average transmittance of 87.35%. Fig. 4k shows the micro-

structure of the hydrogel adhesive patches, which feature distinctive layered structures.

### 3.5 Biocompatibility assessment

After coculturing with L929 cells for a certain period, the cells were subjected to live/dead staining, and the viability status of the cells was observed using inverted fluorescence microscopy (Fig. 5a). Furthermore, the cell viability of the different groups was compared by statistically analyzing the absorbance values obtained from the CCK-8 assay (Fig. 5b). Compared to the control group, all groups with the addition of materials exhibited significantly greater cell viability. Under fluorescence microscopy, numerous green fluorescent live cells were observed in all groups, and the area of green fluorescence in the material groups was similar to that in the control group, with almost no red fluorescence representing dead cells (Fig. 5c). This finding indicates that the materials used in this study demonstrate excellent biocompatibility within the biological system.

Analysis of the hemolysis rate (Fig. 6a and 6b) demonstrated that both the CS hydrogel and C-PDMA patch had hemolysis rates less than 5%, indicating good blood compatibility. To further evaluate the *in vivo* biocompatibility of the chitosan hydrogel adhesive patch, we compared inflammation *in vivo* in rats implanted with the CS hydrogel and the C-PDMA patch (Fig. 6c). The samples were implanted subcutaneously on the backs of the rats. Tissues were collected and subjected to histological analysis at the 14-d time point, and the thickness of the fibrous capsule surrounding the implants



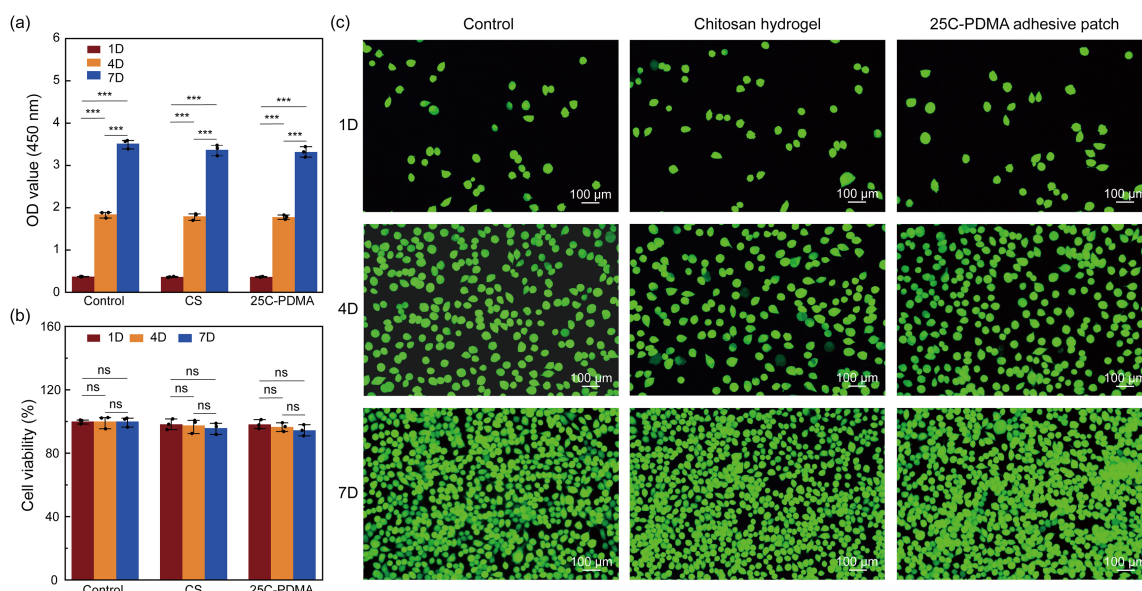


**Fig. 5.** Biocompatibility and cytotoxicity studies. (a, b) OD value and cell viability analysis within 7 d by CCK-8 assay. (c) Live/dead staining images of cells cultured in the hydrogel and control groups after 7 d; scale bar: 100 μm. The values represent the means ± SDs ( $n = 3$ ). The statistical significance was determined using one-way ANOVA; ns, not significant; \*\*\*,  $P \leq 0.001$ .

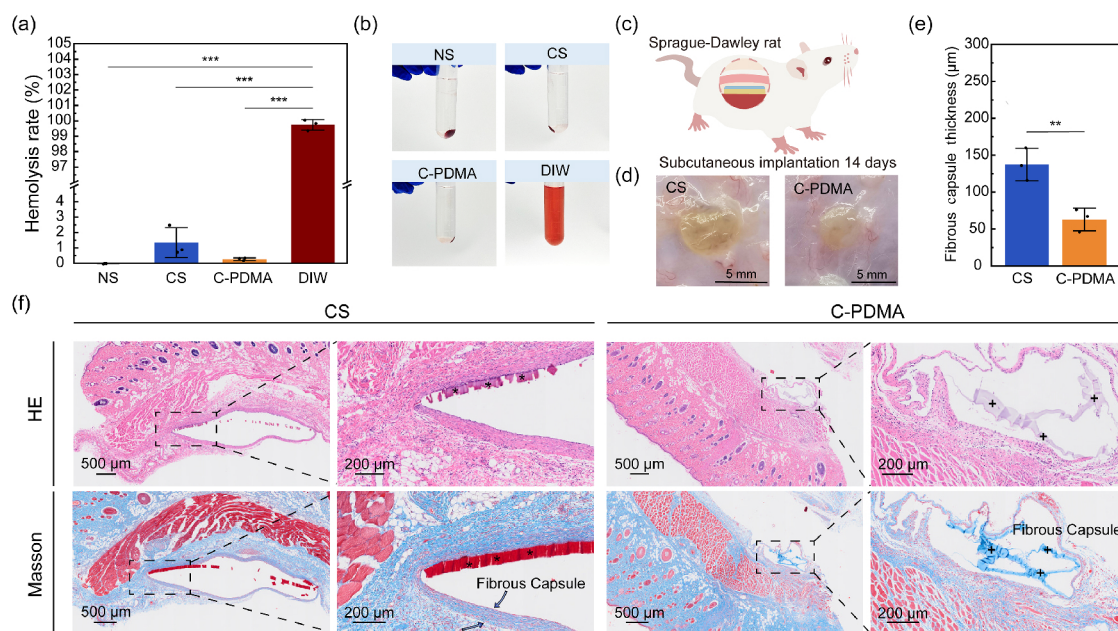


**Fig. 6.** In vivo biocompatibility. (a, b) Hemolysis rates and corresponding images of different materials, with NS indicating normal saline. (c) Rat subcutaneous inflammation model. (d) Macroscopic images of subcutaneous samples from rats. (e) Fibrous capsule thickness around the implanted samples after in vivo implantation. (f) Histological images were stained with HE and Masson's trichrome at 14 d for CS and C-PDMA, with \* representing implant CS and + representing implant C-PDMA. The values represent the means ± SDs ( $n = 3$ ). The statistical significance was determined using the  $t$  test and one-way ANOVA; ns, not significant; \*\*,  $P \leq 0.01$ ; \*\*\*,  $P \leq 0.001$ .

was measured (Fig. 6e). Pathological evaluation revealed only mild erythema or local congestion, indicating a range of “very mild” to “mild” inflammation, as shown in Fig. 6d. At 14 d postimplantation, the thickness of the fibrous capsule was reduced in both groups, with the 14-d C-PDMA group exhibiting the thinnest capsule and the least intense inflammatory

response. HE- and Masson-stained tissue sections of the implanted CS hydrogel and C-PDMA patch (Fig. 6f), respectively, revealed that the inflammation level was slightly greater in the CS hydrogel group than in the C-PDMA patch group. These results suggest that multilayer patches induce low levels of acute and chronic inflammation.

## 4 Conclusions

In conclusion, this study reported a novel chitosan hydrogel adhesive patch with a PDMA and gelatin adhesive layer and chitosan hydrogel backing. By harnessing the synergistic effect of photopolymerization and ANP nanoglue, the C-PDMA patch demonstrated strong adhesion to tissues. The experimental results demonstrated that the chitosan hydrogel adhesive patch exhibited an adhesive energy of 282 J/m<sup>2</sup> to biological tissues in vitro, along with a burst pressure of 450 mmHg. The patch displayed remarkable mechanical properties, including a tensile strength of 4.3 MPa, an elongation rate of 65%, and a fracture toughness of 3.82 MPa. Additionally, the patch showed high transparency and excellent biocompatibility.

Given their exceptional tissue adhesion, mechanical properties, and biocompatibility, nanohectic-based chitosan hydrogel adhesive patches exhibit significant potential for medical applications. It can be utilized not only for tissue repair but also as a solid material foundation for advancements in clinical surgery. Future research endeavors can focus on optimizing its adhesive performance and biocompatibility to address wider clinical needs, thereby facilitating its practical application and commercialization within the medical field.

## Acknowledgements

This work was supported by the Fundamental Research Funds for the Central Universities (WK2060000033) and the China Postdoctoral Science Foundation (2021M703067).

## Conflict of interest

The authors declare that they have no conflict of interest.

## Biographies

**Qing Luo** is currently pursuing a master's degree at the School of Materials Science and Engineering, Zhejiang University of Technology. Her research mainly focuses on the functional design of biomimetic materials and nanoadhesives.

**Dong-Quan Liu** received his master's degree in Clinical Medicine (Surgery) from Chongqing Medical University in 2016. He is currently working in the Department of Hepatobiliary Surgery at Anhui No.2 Provincial People's Hospital. His primary research focuses on liver cancer.

**Liang Dong** received his Ph.D. degree in Biomaterials from the University of Science and Technology of China in 2014. He is currently a researcher at the Hangzhou Institute of Medicine, Chinese Academy of Sciences. His primary research focuses on designing functional biomimetic biomaterials and exploring their biomedical applications, which include tumor treatment, tissue repair, imaging diagnosis, and immunoregulation.

## References

- [1] Wang S Y, Liu J Y, Wang L C, et al. Underwater adhesion and anti-swelling hydrogels. *Advanced Materials Technologies*, **2023**, 8 (6): 2201477.
- [2] Liu X, Liu J, Lin S, et al. Hydrogel machines. *Materials Today*, **2020**, 36: 102–124.
- [3] Yang D Y. Recent advances in hydrogels. *Chemistry of Materials*,

**2022**, 34 (5): 1987–1989.

- [4] Yang J, Yu H J, Wang L, et al. Advances in adhesive hydrogels for tissue engineering. *European Polymer Journal*, **2022**, 172: 111241.
- [5] Du X C, Liu Y J, Yan H Y, et al. Anti-infective and pro-coagulant chitosan-based hydrogel tissue adhesive for sutureless wound closure. *Biomacromolecules*, **2020**, 21 (3): 1243–1253.
- [6] Salzlechner C, Haghighi T, Huebscher I, et al. Adhesive hydrogels for maxillofacial tissue regeneration using minimally invasive procedures. *Advanced Healthcare Materials*, **2020**, 9 (4): 1901134.
- [7] Shen C, Li Y J, Meng Q. Adhesive polyethylene glycol-based hydrogel patch for tissue repair. *Colloids and Surfaces B: Biointerfaces*, **2022**, 218: 112751.
- [8] Liu R X, Li Y B, Chen J C, et al. The preparation of multifunction chitosan adhesive hydrogel by “one-step” method. *Journal of Biomaterials Science, Polymer Edition*, **2020**, 31 (15): 1925–1940.
- [9] Qi P, Zheng Y G, Ohta S, et al. In situ fabrication of double-layered hydrogels via spray processes to prevent postoperative peritoneal adhesion. *ACS Biomaterials Science & Engineering*, **2019**, 5 (9): 4790–4798.
- [10] Luneva O, Olekhovich R, Uspenskaya M. Bilayer hydrogels for wound dressing and tissue engineering. *Polymers*, **2022**, 14 (15): 3135.
- [11] Tang L, Xu Y, Liu F, et al. Synchronous ultraviolet polymerization strategy to improve the interfacial toughness of bilayer hydrogel actuators. *Macromolecules*, **2023**, 56 (16): 6199–6207.
- [12] Chen Q, Zhang X Y, Chen K, et al. Bilayer hydrogels with low friction and high load-bearing capacity by mimicking the oriented hierarchical structure of cartilage. *ACS Applied Materials & Interfaces*, **2022**, 14 (46): 52347–52358.
- [13] Liu J Z, Miao J K, Zhao L, et al. Versatile bilayer hydrogel for wound dressing through PET-RAFT polymerization. *Biomacromolecules*, **2022**, 23 (3): 1112–1123.
- [14] Peng W, Liu C, Lai Y J, et al. An adhesive/anti-adhesive Janus tissue patch for efficient closure of bleeding tissue with inhibited postoperative adhesion. *Advanced Science*, **2023**, 10 (21): 2301427.
- [15] Yao H, Wang C C, Zhang Y C, et al. Manufacture of bilayered composite hydrogels with strong, elastic, and tough properties for osteochondral repair applications. *Biomimetics*, **2023**, 8 (2): 203.
- [16] Li Y, Fu R Z, Duan Z G, et al. Mussel-inspired adhesive bilayer hydrogels for bacteria-infected wound healing via NIR-enhanced nanozyme therapy. *Colloids and Surfaces B: Biointerfaces*, **2022**, 210: 112230.
- [17] Peers S, Montebault A, Ladavière C. Chitosan hydrogels for sustained drug delivery. *Journal of Controlled Release*, **2020**, 326: 150–163.
- [18] Sapru S, Das S, Mandal M, et al. Sericin-chitosan-glycosaminoglycans hydrogels incorporated with growth factors for in vitro and in vivo skin repair. *Carbohydrate Polymers*, **2021**, 258: 117717.
- [19] Liu F L, Wang L, Zhai X R, et al. A multi-functional double cross-linked chitosan hydrogel with tunable mechanical and antibacterial properties for skin wound dressing. *Carbohydrate Polymers*, **2023**, 322: 121344.
- [20] Nakan U, Biekerhazhi S, Tolkyn B, et al. Synthesis, characterization and antibacterial application of copolymers based on *N,N*-dimethyl acrylamide and acrylic acid. *Materials*, **2021**, 14 (20): 6191.
- [21] Bai C Z, Huang Q H, Zhang X, et al. Mechanical strengths of hydrogels of poly(*N,N*-dimethylacrylamide)/alginate with IPN and poly(*N,N*-dimethylacrylamide)/chitosan with semi-IPN microstructures. *Macromolecular Materials and Engineering*, **2019**,

- 304 (11): 1900309.
- [22] Bashir S, Hina M, Ramesh S, et al. Flexible and self-healable poly(*N,N*-dimethylacrylamide) hydrogels for supercapacitor prototype. *Colloids and Surfaces A: Physicochemical and Engineering Aspects*, **2021**, 617: 126377.
  - [23] Suresh D, Suresh A, Kannan R. Engineering biomolecular systems: Controlling the self-assembly of gelatin to form ultra-small bioactive nanomaterials. *Bioactive Materials*, **2022**, 18: 321–336.
  - [24] Yan J, Li S Q, Chen G P, et al. Formation, physicochemical properties, and comparison of heat- and enzyme-induced whey protein-gelatin composite hydrogels. *Food Hydrocolloids*, **2023**, 137: 108384.
  - [25] Yuan X M, Zhu Z, Xia P C, et al. Tough gelatin hydrogel for tissue engineering. *Advanced Science*, **2023**, 10 (24): 2301665.
  - [26] Pan Z, Fu Q Q, Wang M H, et al. Designing nanohesives for rapid, universal, and robust hydrogel adhesion. *Nature Communications*, **2023**, 14 (1): 5378.
  - [27] Weber M, Steinle H, Golombek S, et al. Blood-contacting biomaterials: *in vitro* evaluation of the hemocompatibility. *Frontiers in Bioengineering and Biotechnology*, **2018**, 6: 99.